

# Fluctuation relations for anisotropic systems

Rodrigo Villavicencio-Sanchez,<sup>1,\*</sup> Rosemary J. Harris,<sup>1,†</sup> and Hugo Touchette<sup>2,3,‡</sup>

<sup>1</sup>*School of Mathematical Sciences, Queen Mary University of London, London E1 4NS, UK*

<sup>2</sup>*National Institute for Theoretical Physics (NITheP), Stellenbosch 7600, South Africa*

<sup>3</sup>*Institute of Theoretical Physics, University of Stellenbosch, Stellenbosch 7600, South Africa*

(Dated: September 27, 2018)

Currents of particles or energy in driven nonequilibrium steady states are known to satisfy certain symmetries, referred to as fluctuation relations, determining the ratio of the probabilities of positive fluctuations to negative ones. A generalization of these fluctuation relations has been proposed recently for extended nonequilibrium systems of dimension greater than one, assuming, crucially, that they are isotropic [P. I. Hurtado, C. Pérez-Espigares, J. J. del Pozo, and P. L. Garrido, Proc. Nat. Acad. Sci. (USA) **108**, 7704 (2011)]. Here we relax this assumption and derive a fluctuation relation for  $d$ -dimensional systems having anisotropic bulk driving rates. We illustrate this anisotropic fluctuation relation for the particle current fluctuations in the  $2-d$  anisotropic zero-range process, using both exact and fluctuating hydrodynamic approaches.

PACS numbers: 02.50.-r, 05.40.-a, 05.70.Ln

Fluctuations play an important role at small and mesoscopic scales, for example in nano-devices, chemical reactions, and molecular motors [1–4]. Depending on the properties of the medium and applied forces considered (e.g., the shape of a trapping potential or the spatial distribution of a reactant), such fluctuations may be isotropic or anisotropic and often show certain symmetry properties, such as the *Gallavotti-Cohen fluctuation relation* (GCFR), which has been the subject of considerable theoretical and experimental study [5–9]. The GCFR applies to scalar observables of driven nonequilibrium systems and implies the following relation between positive and negative fluctuations integrated over a time  $t$ :

$$\lim_{t \rightarrow \infty} -\frac{1}{t} \log \frac{P(-A, t)}{P(A, t)} = cA. \quad (1)$$

Here  $P(A, t)$  denotes the probability density function (pdf) of the time-averaged observable  $A$  and  $c$  is a time-independent constant. This relation has been derived for many nonequilibrium observables, including the entropy production of chaotic systems, integrated currents in interacting particle models, and work- or heat-like quantities defined in the context of driven Langevin equations [10–13]. The GCFR has also been verified experimentally, e.g., in turbulent fluids [14] and for manipulated Brownian particles [15, 16].

Recently, Hurtado *et al.* [17] have proposed a generalization of the GCFR, called the *isometric fluctuation relation* (IFR), in an effort to uncover new fluctuation symmetries for higher-dimensional systems. Instead of considering positive and negative fluctuations of scalar observables, their IFR focuses on the current vector  $\mathbf{J}$  of  $d$ -dimensional nonequilibrium systems and implies that any two currents  $\mathbf{J}'$  and  $\mathbf{J}$  of equal magnitude,  $|\mathbf{J}'| = |\mathbf{J}|$ , obey the following relation:

$$\lim_{t \rightarrow \infty} -\frac{1}{t} \log \frac{P(\mathbf{J}', t)}{P(\mathbf{J}, t)} = \mathbf{E} \cdot (\mathbf{J} - \mathbf{J}'), \quad (2)$$

where  $\mathbf{E}$  is a  $d$ -dimensional constant field conjugate to  $\mathbf{J}$ . This relation can be derived from the hydrodynamic fluctuation theory and has been shown to hold so far for several important nonequilibrium models, including the boundary-driven  $2-d$  Kipnis-Marchioro-Presutti (KMP) process and a hard-disk fluid model [17].

Crucially, both the derivation and the application of the IFR rely on the systems of interest being isotropic. Our goal here is to remove this assumption so as to derive a fluctuation relation similar to (2) but which applies to more general systems having anisotropic diffusive dynamics. As a test of this anisotropic fluctuation relation (AFR), we consider the  $2-d$  zero-range process on a square lattice with different hopping rates in  $x$ - and  $y$ -directions. We obtain the current fluctuations in this model from the hydrodynamic fluctuation theory as well as exactly from the microscopic definition of the process. Significantly, this allows us to study convergence and check the hydrodynamic theory predictions in a precise and controlled way for system sizes up to  $10^5 \times 10^5$  sites, much larger than currently accessible in simulations.

*Hydrodynamic formalism and IFR.*— We study diffusive lattice gases evolving on a  $d$ -dimensional (hypercubic) lattice of side  $L$ . In the macroscopic scaling limit, these systems are described, following the hydrodynamic fluctuation theory [18–21], by a local particle density  $\rho(\mathbf{r}, t)$ , with  $\mathbf{r} \in \Omega = [0, 1]^d$ , and a local current

$$\mathbf{j}(\mathbf{r}, t) = -D(\rho)\nabla\rho(\mathbf{r}, t) + \boldsymbol{\xi}(\mathbf{r}, t). \quad (3)$$

Density boundary conditions account physically for the interaction with reservoirs while mass conservation imposes the continuity equation

$$\partial_t \rho(\mathbf{r}, t) = -\nabla \cdot \mathbf{j}(\mathbf{r}, t). \quad (4)$$

The local current  $\mathbf{j}(\mathbf{r}, t)$  is composed of two parts: a deterministic drift with a density-dependent *diffusivity*

$D(\rho)$ , representing the hydrodynamic (noiseless) evolution of the model, and a random noise  $\boldsymbol{\xi}(\mathbf{r}, t)$ , accounting for the fluctuations of the model around its hydrodynamic behavior. This noise is assumed to be a space-time white noise with covariance  $L^{-d}\sigma(\rho)\delta(\mathbf{r}'-\mathbf{r})\delta(t'-t)$ , where  $\sigma(\rho)$  is the density-dependent *mobility*. To allow for any anisotropy in the system,  $\sigma(\rho)$  and  $D(\rho)$  are here taken to be  $d \times d$  matrices rather than scalar functions.

The nonequilibrium state of the model is characterized by the *global current* averaged over time  $t$ ,

$$\mathbf{J} = \frac{1}{t} \int_0^t d\tau \int_{\Omega} d\mathbf{r}' \mathbf{j}(\mathbf{r}', \tau). \quad (5)$$

For some choices of boundary conditions and matrices  $D$  and  $\sigma$ ,  $\mathbf{J}$  converges in the long-time limit,  $tL^d \rightarrow \infty$ , to a typical value, corresponding to the hydrodynamic current. Here we are interested in fluctuations of  $\mathbf{J}$  about this limit and in any symmetries satisfied by its stationary pdf  $P(\mathbf{J}, t)$ . In most cases, this pdf has an exponential form in  $t$  and  $L^d$ ,

$$P(\mathbf{J}, t) = e^{-tL^d \hat{e}(\mathbf{J}) + o(tL^d)}, \quad (6)$$

which is referred to as a large deviation principle [22]. The rate function  $\hat{e}(\mathbf{J})$  characterizes the speed at which  $P(\mathbf{J}, t)$  converges to its typical value, and so quantifies the asymptotic probability of rare current fluctuations.

From a microscopic point of view, current and density fluctuations are linked. In the hydrodynamic limit, it can be shown that a given value of the global current  $\mathbf{J}$  is overwhelming likely to be realized by particular spatiotemporal profiles of the local density and current, referred to as *optimal* profiles. These optimal profiles and the corresponding rate function  $\hat{e}(\mathbf{J})$  are obtained within a path integral formalism by an asymptotically exact ‘‘saddle-point’’ calculation over all realizations of the noise which yield local currents (3) consistent with the desired global value  $\mathbf{J}$ .

Following this picture, the IFR of (2) was derived in [17] under the following assumptions: (i) isotropic diffusivity and mobility (i.e.,  $D(\rho)$  and  $\sigma(\rho)$  proportional to the identity matrix), (ii) time-independent optimal profiles for both current and density, (iii) optimal density profiles with spatial structure only in the direction of driving (namely, constant perpendicular to the field), and (iv) optimal current profiles *without* spatial structure (i.e., constant local current). Underlying the IFR is the remarkable property that the optimal density profile is the same for all currents  $\mathbf{J}$  on a *circle* of given radius around the origin. Our contribution is to address the same problem but, significantly, without assuming the isotropic condition (i). This generalization leads to breakdown of the IFR even for small fluctuations.

*Anisotropic fluctuation relation.*— We now aim to determine which currents can be related via a fluctuation relation of the same type as (2). We assume that the

diffusive system has open boundary conditions in the  $x$ -direction, without loss of generality, and periodic boundary conditions in the other  $(d-1)$  directions. From the macroscopic fluctuation theory outlined above, the rate function of  $\mathbf{J}$  is obtained from the following minimization problem [18–21]:

$$\hat{e}(\mathbf{J}) = \min_{\rho, \mathbf{j}} \frac{1}{t} \int_0^t d\tau \int_{\Omega} d\mathbf{r} \mathcal{L}(\tau, \mathbf{r}, \rho, \nabla \rho), \quad (7)$$

involving the Lagrangian

$$\mathcal{L}(\tau, \mathbf{r}, \rho, \nabla \rho) = \frac{(\mathbf{j}(\mathbf{r}, \tau) + D\nabla \rho)^T \Sigma (\mathbf{j}(\mathbf{r}, \tau) + D\nabla \rho)}{4}. \quad (8)$$

This is a constrained minimization problem over all local densities and currents related by the continuity equation (4) and satisfying the boundary conditions. The local density and current solving the minimization are the optimal profiles mentioned above. Here  $\Sigma$  is the diagonal matrix with elements  $\Sigma_{kk} = \sigma_k^{-1}$ , where  $\sigma_k$  is the mobility in the  $k$ th direction. Similarly, the diffusivity  $D(\rho)$  is a diagonal matrix with elements  $D_k$ .

The constrained minimization (7) is difficult to solve in general. However, following [17], it can be simplified under the hypotheses (ii) and (iv) above to obtain

$$\hat{e}(\mathbf{J}) = \min_{\rho} \frac{1}{4} \int d\mathbf{r} (\mathbf{J} + D\nabla \rho)^T \Sigma (\mathbf{J} + D\nabla \rho). \quad (9)$$

The associated Euler-Lagrange equation is then

$$\sum_{k=1}^d \frac{2D_k \rho_{x_k}^2 \partial_{\rho} D_k + 2D_k^2 \rho_{x_k}^{(2)}}{4\sigma_k} - \frac{(D_k^2 \rho_{x_k}^2 - J_k^2) \partial_{\rho} \sigma_k}{4\sigma_k^2} = 0, \quad (10)$$

where we have used the notation  $\rho_{x_k}^{(n)} = \partial^n \rho / \partial x_k^n$ .

Now we use (iii), consistent with our chosen boundary conditions, to equate the terms  $2D_k^2 \rho_{x_k}^{(2)}$  and  $D_k^2 \partial_{\rho} \rho_{x_k}^2$ . Integrating (10), we find that the density profile that minimizes the functional (9) is given by the first-order differential equation

$$(D\nabla \rho)^T \Sigma (D\nabla \rho) = \mathbf{J}^T \Sigma \mathbf{J} + 4C, \quad (11)$$

where  $C$  is a constant of integration. Then, noting that for diffusive lattice gases we have [12, 13]

$$\mathbf{E} = 2 \int_{\Omega} d\mathbf{r} \Sigma D \nabla \rho, \quad (12)$$

we obtain with (9) and (11), the relation

$$\hat{e}(\mathbf{J}) - \hat{e}(\mathbf{J}') = \mathbf{E} \cdot (\mathbf{J}' - \mathbf{J}), \quad (13)$$

for global currents satisfying

$$\mathbf{J}^T \Sigma \mathbf{J} = \mathbf{J}'^T \Sigma \mathbf{J}'. \quad (14)$$

The two equations above define our anisotropic generalization of the IFR, called AFR, showing that the relation

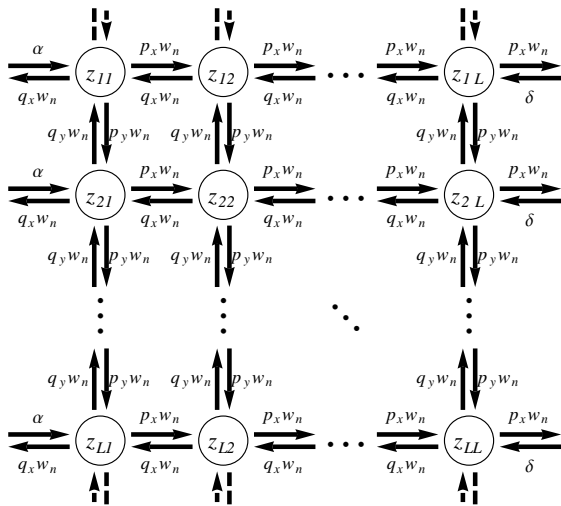


FIG. 1. 2-d ZRP with anisotropic hopping rates. Input rates  $\alpha$  and  $\delta$  determine particle reservoir densities in the  $x$ -direction. Periodic boundary conditions in the  $y$ -direction.

of Eq. (2) is now valid for currents on *ellipses* determined by (14), rather than the circles obtained in [17] for  $\Sigma$  proportional to the identity matrix. Similarly, generalizing the underlying structure, we also see from Eq. (11) that currents on a given ellipse arise from the same optimal density profile. In other words, optimal density profiles are invariant on ellipses, with principal axes determined by the anisotropy.

*Zero-range process.*— We now present a test of the AFR (13) for an anisotropic zero-range process (ZRP) on an  $L \times L$  square lattice. In this model, each site may be occupied by any number of particles, the top-most of which jumps randomly to a neighboring site after an exponentially-distributed waiting time. Figure 1 shows the transition rates: they are determined by an interaction factor  $w_n$ , which depends only on the number  $n$  of particles on the departure site, multiplied by hopping rates for the different jump directions and boundaries. Here we choose symmetric hopping rates,  $p_x = q_x$  and  $p_y = q_y$ , which implies that the system scales as a diffusive process in the hydrodynamic limit ( $L \rightarrow \infty$ ). We also take boundary rates in the  $x$ -direction corresponding to reservoir densities  $\rho_L$  and  $\rho_R$ , with  $\rho_L > \rho_R$ , to induce a rightwards mean current. A feature of this model is that, depending on the choice of the term  $w_n$ , the system may show a condensation phase transition where particles accumulate on one or more sites [23]. Indeed, even with a well-defined steady state, a bounded  $w_n$  (i.e.,  $\lim_{n \rightarrow \infty} w_n = a$  with  $a < \infty$ ) results in instantaneous condensation for large current fluctuations [24].

*ZRP-Hydrodynamic limit.*— The mobility and diffusion coefficients of the ZRP in each direction are  $\sigma_k = p_k z(\rho)$  and  $D_k = p_k z'(\rho)$  [18, 25, 26]. Here  $z(\rho)$  is

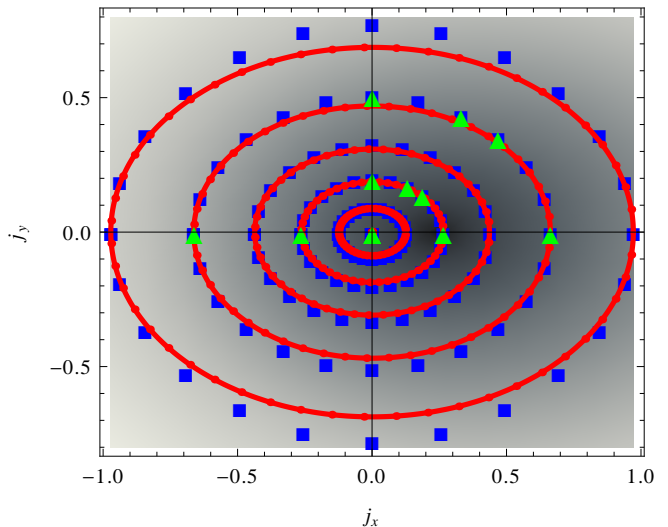


FIG. 2. Current rate function for ZRP with interaction  $w_n = 1$  and boundary densities  $\rho_L = 1/2$  and  $\rho_R = 1/10$ . Shaded background: magnitude of  $\hat{e}(\mathbf{J})$  calculated in hydrodynamic approach (darkest at minimum). Solid lines: currents satisfying the AFR. Blue squares: points of constant  $e(\boldsymbol{\lambda})$  mapped to current space for system of  $L = 10^5$ .

a fugacity parameter connected to the density by  $\rho = z \partial (\log \mathcal{Z}) / \partial z$ , where  $\mathcal{Z}$  plays the role of a grand canonical partition function. The form of  $\mathcal{Z}$  depends on  $w_n$ , e.g., choosing  $w_n = w$ , we have  $\sigma_x/p_x = \sigma_y/p_y = w\rho(\rho+1)^{-1}$  and  $D_x/p_x = D_y/p_y = w(\rho+1)^{-2}$ . In this case, we can explicitly solve Eq. (11) to find the optimal density profile and then (9) to find the current rate function  $\hat{e}(\mathbf{J})$ . A similar calculation can be done for  $w_n = n$ , which corresponds to non-interacting particles. In both cases, the results confirm that the currents satisfying the AFR (13) are located on ellipses verifying (14). This is shown for the interacting case  $w_n = 1$  in Fig. 2 with hopping rates  $p_x = 1$  and  $p_y = 1/2$ . Moreover, the optimal density profile associated with currents on each ellipse is invariant, a non-trivial result which follows again from (11).

The specific shape of the optimal density profile depends on the current fluctuation considered, as shown in Fig. 3, again for the case  $w_n = 1$ . We observe that the non-linearity of Eq. (11) results in two different kinds of density profile: for small fluctuations, the density is maximal at the left boundary and decreases monotonically, whereas for large fluctuations, the maximum density occurs at a point  $x_{\max}$  between the two boundaries. For  $w_n = w$ , the density at  $x_{\max}$  diverges at a critical current given by  $|\Sigma \mathbf{J}_c| = K$  where  $K$  can be explicitly calculated. This is the signature of the condensation mentioned above. The present analysis does not address the probability of current fluctuations outside this ellipse; indeed, as for the GCFR and IFR, we do not expect our AFR to hold in this regime, cf. [27].

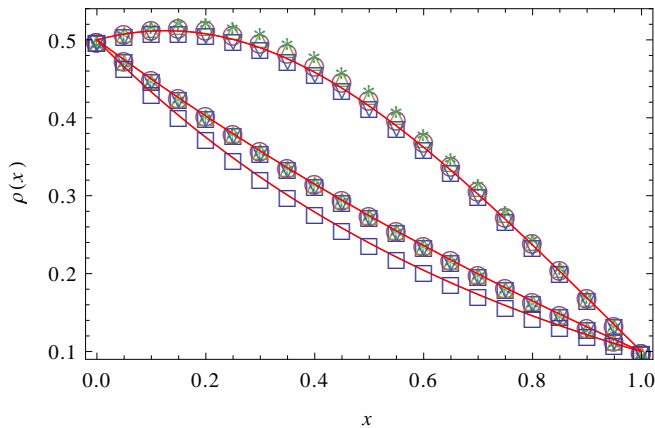


FIG. 3. Optimal density profiles for currents on ellipses of Fig. 2, increasing magnitude from bottom to top. Solid lines: hydrodynamic theory; Symbols: results for  $10^5 \times 10^5$  lattice at currents marked by green triangles in Fig. 2, angles from  $x$ -axis are 0 ( $\square$ ),  $\pi/4$  ( $\circ$ ),  $\pi/3$  ( $\triangle$ ),  $\pi/2$  ( $*$ ),  $\pi$  ( $\nabla$ ).

*ZRP-microscopic approach.*— Remarkably, it is possible to obtain exact results for the fluctuations of the current  $\mathbf{J}$  in the ZRP for any lattice size and any interaction  $w_n$ , providing a precise test of the AFR and the validity of the assumptions behind it. These results follow by calculating the so-called *scaled cumulant generating function* (SCGF),

$$e(\boldsymbol{\lambda}) = \lim_{t \rightarrow \infty} -\frac{1}{tL^d} \log \langle e^{-tL^d \boldsymbol{\lambda} \cdot \mathbf{J}} \rangle, \quad (15)$$

where  $\langle \cdot \rangle$  denotes the expectation value. This function can be explicitly calculated by writing the Master equation analogously to a quantum Schrödinger equation [28] and extracting  $e(\boldsymbol{\lambda})$  as the lowest eigenvalue of some modified Hamiltonian. The optimal density profile is then obtained from the corresponding eigenvector. In practice, this involves solving an  $L \times L$  system of linear equations for modified fugacities as a function of  $\boldsymbol{\lambda}$ . From  $e(\boldsymbol{\lambda})$ , we can verify the AFR either by obtaining the rate function  $\hat{e}(\mathbf{J})$  as the Legendre transform of  $e(\boldsymbol{\lambda})$  or by noticing that Eq. (13) translates into the symmetry,

$$e(\boldsymbol{\lambda} + \mathbf{E}) = e(\boldsymbol{\lambda}' + \mathbf{E}), \quad (16)$$

where the vectors  $\boldsymbol{\lambda}$  and  $\boldsymbol{\lambda}'$  satisfy

$$(\boldsymbol{\lambda} + \mathbf{E})^T \sigma(\boldsymbol{\lambda} + \mathbf{E}) = (\boldsymbol{\lambda}' + \mathbf{E})^T \sigma(\boldsymbol{\lambda}' + \mathbf{E}). \quad (17)$$

Geometrically, this means that  $e(\boldsymbol{\lambda})$  is constant for vectors  $\boldsymbol{\lambda}$  located on ellipses around the field  $\mathbf{E}$ . These ellipses are related by Legendre transform to those seen for the current in Fig. 2.

Note that the modified fugacities involved in the microscopic solution have no explicit dependence on  $w_n$  facilitating the solution for any form of realistic interaction. However,  $w_n$  does control the relation between

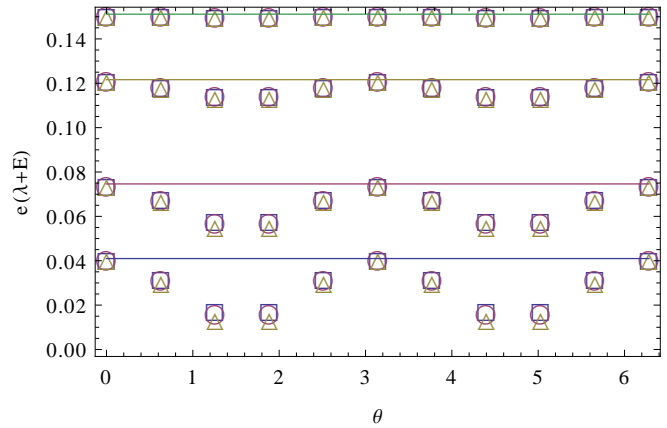


FIG. 4. AFR for ZRP with  $w_n = n$  (boundary conditions  $\rho_L = 1/2$  and  $\rho_R = 1/10$ ). Hydrodynamic limit of SCGF expected to be constant for  $\boldsymbol{\lambda}$  on ellipses around field  $-\mathbf{E}$ . Solid lines: hydrodynamic prediction. Empty shapes: scaled microscopic results for lattice sizes: 32 ( $\triangle$ ), 100 ( $\circ$ ),  $10^5$  ( $\square$ ).

fugacity and density and, importantly, determines the current regime in which the SCGF is given by the calculated lowest eigenvalue and the fluctuation relation is expected to hold. For example, in the case  $w_n = 1$  we can numerically calculate the maximum current before condensation, finding a bound consistent with the hydrodynamic approach.

The result of the Legendre transform of the ellipses of constant  $e(\boldsymbol{\lambda})$  for the case  $w_n = 1$  is shown as data points in Fig. 2 for the largest size we studied,  $L = 10^5$ . There we see a good agreement between the microscopic and hydrodynamic approaches, especially for small current magnitudes and for angles near the forward and backwards currents (i.e., approximately along and opposite to the field direction), confirming the AFR for these currents. There are some discrepancies for large fluctuations perpendicular to the field; we shall discuss below their possible significance.

Using the microscopic solution of the model, we can also examine the underlying structure of the optimal density profiles. In Fig. 3, we compare the resulting optimal density profiles for increasing currents using microscopic and hydrodynamic theories. For  $10^5 \times 10^5$  sites, the density profiles of forward and backward currents appear to match exactly with the hydrodynamic result, whereas for large fluctuations in other directions there are some deviations.

To look in more detail at these differences and the convergence of the microscopic results to the hydrodynamic limit, it is convenient to study whether Eqs. (16) and (17) obtained from the hydrodynamic theory are satisfied for the microscopic  $e(\boldsymbol{\lambda})$  – see Fig. 4 for the case of non-interacting particles. As expected, for small current fluctuations, the microscopic results approach the hydro-

dynamic prediction as the system size increases. For large fluctuations, however, they appear to converge only for angles along and opposite the field, not angles perpendicular to it. Similar discrepancies were seen in simulations of the KMP-process for system size  $L = 32$  [17] and, in that case, were interpreted as a finite-size effect.

Our exact results, obtained for the much larger size of  $L = 10^5$ , open up the possibility that the microscopic results do not actually converge to the hydrodynamic prediction for directions normal to the field. One possible explanation for this could be that assumption (*iv*) used in the hydrodynamic derivation is not exactly satisfied by the ZRP. Significantly, this assumption is not made in the microscopic analysis; we implicitly use only assumptions (*ii*) and (*iii*) which together imply the weaker condition that the optimal current is divergence free and has no structure perpendicular to the field, i.e., in the  $y$ -direction here. Indeed, for models such as the ZRP having a density-dependent mobility, one expects physically that an  $x$ -dependent density profile might lead to the  $y$ -component of the current also having an  $x$ -dependence, which would violate assumption (*iv*). This is supported by the observation that, when the optimal density profile is approximately constant (e.g., close to equilibrium  $\rho_L = \rho_R$ ), the microscopic and hydrodynamic results seem to converge.

*Conclusion.*— We have presented in this paper an extension of the recently-introduced IFR to diffusive systems having anisotropic driving rates. This AFR shows very good agreement with exact microscopic calculations for small current fluctuations, as well as for large currents close to the driving field. This is particularly relevant, since it allows the symmetry to be efficiently probed experimentally (say, for manipulated Brownian particles with anisotropy) without the need to measure rare backward fluctuations. Moreover, from a theoretical point of view, the observation that microscopic results for perpendicular current fluctuations may not converge to the AFR sheds light on the underlying physical assumptions (also required for the original IFR). The exactly solvable ZRP provides an ideal testing ground for future work focusing on the precise role of these assumptions.

RVS is supported by the Mexican National Council for Science and Technology (CONACyT) Scholarship scheme. RJH and HT are grateful to the Kavli Institute for Theoretical Physics China, for support and hospitality while this work was being finalized.

- 
- \* sanchez@maths.qmul.ac.uk  
† rosemary.harris@qmul.ac.uk  
‡ htouchette@sun.ac.za
- [1] H. G. Schuster, R. Klages, W. Just, and C. Jarzynski, *Nonequilibrium Statistical Physics of Small Systems: Fluctuation Relations and Beyond* (John Wiley, New York, 2013).
  - [2] C. Bustamante, J. Liphardt, and F. Ritort, *Phys. Today* **58**, 43 (2005).
  - [3] F. Jülicher, A. Ajdari, and J. Prost, *Rev. Mod. Phys.* **69**, 1269 (1997).
  - [4] F. Ritort, in *Advances in Chemical Physics* (John Wiley, New York, 2008) pp. 31–123.
  - [5] C. Maes, *Sem. Poincaré* **2**, 29 (2003).
  - [6] J. Kurchan, *J. Stat. Mech.* **2007**, P07005 (2007).
  - [7] R. J. Harris and G. M. Schütz, *J. Stat. Mech.* **2007**, P07020 (2007).
  - [8] U. Seifert, *Rep. Prog. Phys.* **75**, 126001 (2012).
  - [9] F. Ritort, *Sem. Poincaré* **2**, 192 (2003).
  - [10] D. J. Evans, E. G. D. Cohen, and G. P. Morriss, *Phys. Rev. Lett.* **71**, 2401 (1993).
  - [11] G. Gallavotti and E. G. D. Cohen, *Phys. Rev. Lett.* **74**, 2694 (1995).
  - [12] J. Kurchan, *J. Phys. A: Math. Gen.* **31**, 3719 (1998).
  - [13] J. L. Lebowitz and H. Spohn, *J. Stat. Phys.* **95**, 333 (1999).
  - [14] S. Ciliberto, N. Garnier, S. Hernandez, C. Lacpatia, J.-F. Pinton, and G. R. Chavarría, *Physica A* **340**, 240 (2004).
  - [15] G. M. Wang, E. M. Sevick, E. Mittag, D. J. Searles, and D. J. Evans, *Phys. Rev. Lett.* **89**, 050601 (2002).
  - [16] S. Ciliberto, S. Joubaud, and A. Petrosyan, *J. Stat. Mech.* **2010**, P12003 (2010).
  - [17] P. I. Hurtado, C. Pérez-Espigares, J. J. del Pozo, and P. L. Garrido, *Proc. Nat. Acad. Sci. (USA)* **108**, 7704 (2011).
  - [18] L. Bertini, A. De Sole, D. Gabrielli, G. Jona-Lasinio, and C. Landim, *J. Stat. Phys.* **107**, 635 (2002).
  - [19] L. Bertini, A. De Sole, D. Gabrielli, G. Jona-Lasinio, and C. Landim, *Phys. Rev. Lett.* **94**, 030601 (2005).
  - [20] L. Bertini, A. De Sole, D. Gabrielli, G. Jona-Lasinio, and C. Landim, *J. Stat. Phys.* **123**, 237 (2006).
  - [21] T. Bodineau and B. Derrida, *Phys. Rev. Lett.* **92**, 180601 (2004).
  - [22] H. Touchette, *Phys. Rep.* **478**, 1 (2009).
  - [23] E. Levine, D. Mukamel, and G. Schütz, *J. Stat. Phys.* **120**, 759 (2005).
  - [24] R. J. Harris, A. Rákos, and G. M. Schütz, *J. Stat. Mech.* **2005**, P08003 (2005).
  - [25] A. Masi and P. Ferrari, *J. Stat. Phys.* **36**, 81 (1984).
  - [26] C. Kipnis and C. Landim, *Scaling Limits of Interacting Particle Systems*, Grundlehren der mathematischen Wissenschaften, Vol. 320 (Springer-Verlag, Berlin, 1999).
  - [27] R. J. Harris, A. Rákos, and G. M. Schütz, *Europhys. Lett.* **75**, 227 (2006).
  - [28] G. M. Schütz, in *Phase Transitions and Critical Phenomena*, Vol. 19, edited by C. Domb and J. L. Lebowitz (Academic Press, New York, 2001).